

Train by Reconnect: Decoupling Locations of Weights from their Values

Yushi Qiu Reiji Suda

Graduate School of Information Science and Technology, The University of Tokyo
{yushi621, reiji}@is.s.u-tokyo.ac.jp

Abstract

What makes untrained deep neural networks (DNNs) different from the trained performant ones? By zooming into the weights in well-trained DNNs, we found it is the *location* of weights that hold most of the information encoded by the training. Motivated by this observation, we hypothesize that weights in stochastic gradient-based method trained DNNs can be separated into two dimensions: the locations of weights and their exact values. To assess our hypothesis, we propose a novel method named *Lookahead Permutation* (LaPerm) to train DNNs by reconnecting the weights. We empirically demonstrate the versatility of LaPerm while producing extensive evidence to support our hypothesis: when the initial weights are random and dense, our method demonstrates speed and performance similar to or better than that of regular optimizers, e.g., Adam; when the initial weights are random and sparse (many zeros), our method changes the way neurons connect and reach accuracy comparable to that of a well-trained fully initialized network; when the initial weights share a single value, our method finds weight agnostic neural network with far better-than-chance accuracy.

1 Introduction

Conventional gradient-based algorithms for training deep neural networks (DNNs), such as Stochastic Gradient Descent (SGD), find the appropriate numerical values for a set of predetermined weight vectors θ . These algorithms apply the changes $\Delta\theta$ to θ at each iteration. Denoting the weight vectors at the t -th iteration as θ_t , they use the following update rule: $\theta_t \leftarrow \theta_{t-1} + \Delta\theta_{t-1}$. Therefore, we have the relation between a trained and an untrained DNN: $\theta_T = \theta_0 + \sum_{t=1}^T \Delta\theta_t$, given the initial weights θ_0 and the weights θ_T obtained by training the network for T iterations. However, since $\Delta\theta_t$ is dependent on θ_{t-1} and $\Delta\theta_{t-1}$ for every t , the term $\sum_{t=1}^T \Delta\theta_t$ resembles a black box, i.e., every entry of θ_T can potentially take on any real values, and thus it is unclear what is the most substantial change that the training applied to the initial weights.

In this work, we make a contribution to opening this black box by hypothesizing that weights can be decoupled into two dimensions: the *locations* of weights and their *exact values*. As a result, DNNs can be trained following the same stochastic gradient-based regime but using a fundamentally different update rule: $\theta_t \leftarrow \sigma_t(\theta_{t-1})$, for a permutation operation σ_t . Consequently, we have $\theta_T = \sigma_1(\dots(\sigma_T(\theta_0)))$, and thus have $\theta_T = \sigma_k(\theta_0)$ for σ_k from the same permutation group. We show that, given a properly chosen neural architecture initialized with random weights, while fine tuning the weight values is important for reaching state-of-the-art results, guaranteeing the location of weights plays a crucial role in making neural networks performant.

This paper is structured as follows. In Section 2, we describe an interesting phenomenon in the way weights are distributed in trained DNNs, which cast light on understanding how information is encoded by training. In Section 3, we show that stochastic gradient updates can be translated into “permutations”. In Section 4, we propose a novel algorithm, named *Lookahead Permutation* (LaPerm),

to effectively train DNNs by reconnection. In Section 5, we showcase the versatility of LaPerm in both training and pruning, and revisit and improve our hypothesis based on empirical evidence.

2 Similarity of Weight Profiles

DNNs perform chains of mathematical transformations from their input to output. At the core of these transformations are *feature extractions*. Artificial neurons, the elementary vector-to-scalar functions in neural networks, are where feature extractions take place. The incoming weighted connections of a neuron can be represented using a one-dimensional vector (flatten if it has a higher dimension, e.g., convolutional kernel), which we refer to as a *weight vector*. All neuron connections between two layers can be represented by a *weight matrix*, where each column is a weight vector.

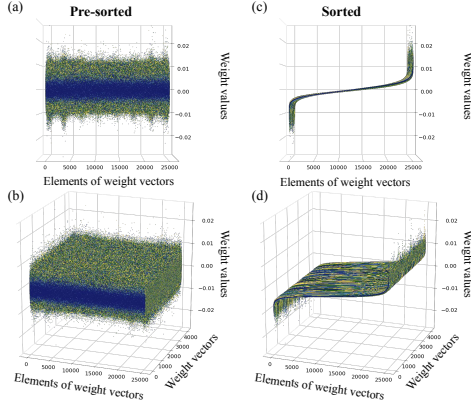


Figure 1: *Profiling* a weight matrix in a pre-trained VGG16 on ImageNet. Figure (a) and (b), Figure (c) and (d) are the same plot in different view angles. Color of each single scatter plot is chosen in order from {midnight-blue, gold, darkgreen, steelblue}, cyclically.

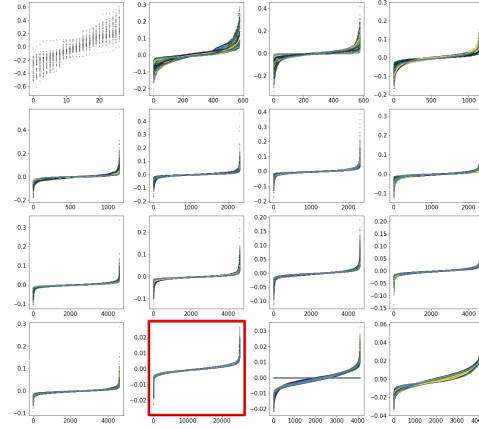


Figure 2: *Profiling* all weight matrices in a pre-trained VGG16. The weight profile selected for Figure 1 is marked red. The z-axes are hidden (similar to in Figure 1 (a) and (b)).

To gain insight on how the information is encoded in a trained DNN, it is natural to begin with observing weight vectors. Here, we visualize a weight matrix by drawing a scatter plot for each of its weight vectors, where the x and y-axis indicate the indices and weight values associated with each entry, respectively. We stack these scatter plots on the same figure along the z-axis, such that all plots share the same x and y-axis. Figure 1 (a) and (b) show such a visualization of a weight matrix from different view angles; it represents all weighted connections between the last convolutional layer and the first fully connected layer in VGG16 [28] pre-trained on ImageNet [5]. At a glance, these plots appear to be roughly zero-meaned, but overall, a jumble of random-looking points. Nothing is particularly noticeable *until we sort all the weight vectors* and redo the plotting to obtain Figure 1 (b) and (c). The patterns shown on these figures imply that *all 4096 weight vectors had almost identical distribution and center* as their scatter plots closely overlap with each other. In forthcoming discussions, we refer to sorted weight vectors as *weight profile*.

As shown in Figure 2, although the shapes may vary, similar patterns are observed in most layers. We also found these patterns in every other tested pre-trained convolutional neural networks (CNNs), such as ResNet50 [10], MobileNet [12] and NASNet [33]. We call this phenomenon of weight vectors associated with a group of neurons possessing strikingly similar statistical properties, the *Similarity of Weight Profiles (SoWP)*. It reveals the beauty and simplicity in how well-trained neural networks extract and store information.

Similarity is where two or more objects lack differentiating features. SoWP implies that many features encoded by training are lost after sorting. In other words, *the features are mostly stored in the pre-sorted orders of the weight vectors*. Consequently, SoWP allows the weights of a well-trained DNN to be near-perfectly separated into two components: the statistics of weight values and their relative orders.

3 Is Permutation the Essence of Learning?

If information can truly be encoded in the relative orders of weights, we would expect the progress of learning to be reflected in the changes of these orders. We train a fully-connected DNN with 2 hidden layers (100 ReLU units each) on MNIST [19]. In isolation, we train using the same architecture and initialization under four different settings: (1) SGD (1e-1) with no regularization. (2) Adam (1e-3) with no regularization. (3) Adam (1e-3) with L2 weight decay [17] and learning rate drops. Full experiment settings are the Appendix. During the training, we extract the orders of weights by focusing on their *rankings* within each weight vector.

The *ranking* of a weight vector w_j is defined as a vector R_j , where $\#R_j = \#w_j$, of distinct integers in $[0, \#w_j)$, such that $w_j[p] > w_j[q]$ implies $R_j[p] > R_j[q]$, for all integers $p, q \in [0, \#w_j)$, $p \neq q$. Here $\#w_j$ denotes the number of elements in w_j ; $w_j[p]$ denotes the p -th element of the vector w_j . If the ranking $R_{j,t}$ of w_j at the t -th iteration is different from $R_{j,t-1}$ at the $t-1$ -th iteration, there must exist a *permutation* σ_t such that $R_{j,t} = \sigma_t(R_{j,t-1})$. Here, we simply compute $D_{j,t} = |R_{j,t} - R_{j,t-1}|$, which we refer to as *ranking distance*. The i -th entry of the ranking distance $D_{j,t}[i]$ indicates the distance of change in the ranking of $w_j[i]$ in the past iteration.

For a weight matrix W , we compute the mean: $\bar{D}_t = \sum_j \sum_i D_{j,t}[i] / \#W$, where $\#W$ is the total number of entries in W , and standard deviation: $SD[D_t] = \sqrt{\sum_j \sum_i (D_{j,t}[i] - \bar{D}_t)^2 / \#W}$ of the ranking distance.

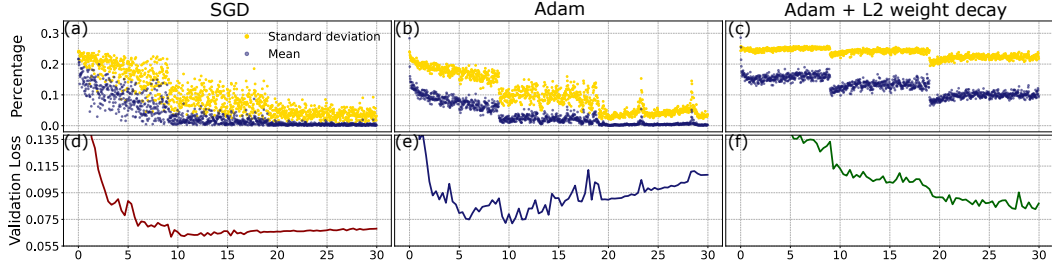


Figure 3: Monitoring ranking distance and validation loss in the first weight matrix of the network. Each column title indicates the experiment setting. Under each title from the top to bottom shows the evolution of the ratio of the mean and standard deviation of the ranking distance to the size of the weight vector, i.e., $\bar{D}_t/784$ and $SD[D_t]/784$, and the trend of validation loss on 10000 test images.

Results & Analysis Here we briefly point out in the results shown in Figure 3 that changes in the ranking reflect the progress of learning. (1) the behaviors of permutations in (a)~(c) showed unique traits under each setting. For setting (1), the trends seem random, especially when the learning rate is 0.1, which reflects how SGD’s updates are largely dependent on the randomly sampled batch d . In contrast, in (b), (c), since Adam’s updates take into account previous gradients, the permutations appear to follow a certain trend. In (c), when L2 weight decay is applied, the change in ranking is significantly greater in both its number and size. It implies that the weights are becoming smaller and closer to each other because of the weight penalties. The closer they are, the easier their rankings can be swapped and the larger ranking distance the swap would cause by an update. Moreover, in (b) and (e) at around the 24 and 29th epoch, the sharp rise in the mean of ranking distance predicted the deterioration in validation loss. The full experiment and analysis are in the Appendix.

4 Lookahead Permutation (LaPerm)

Motivated by the observation in Section 3, we propose *Lookahead Permutation (LaPerm)*, a method to train DNNs by permuting the weighted connections. This method is inspired by the Lookahead (LA) optimizer [31] and Reptile optimizer [25]. A pseudo-code of LaPerm is shown in Algorithm 1.

We consider training a feed-forward network $F_{\theta_0}(x)$ with initial weights $\theta_0 \sim D_\theta$. Before the training starts, LaPerm creates a copy of θ_0 and ascending sorts every weight vector of this copy, then store it as θ_{sorted} . At any step t during training, LaPerm holds onto both θ_{sorted} and θ_t , where θ_{sorted} is served as a preparation for *synchronization* and is maintained as sorted throughout training; θ_t is used as a reference to permute θ_{sorted} , which is updated regularly at each mini-batch using an inner optimizer Opt of choice, e.g., Adam.

Synchronization Once every k steps, *synchronization*: $\theta_t \leftarrow \sigma_{\theta_t}(\theta_{\text{sorted}})$ is performed, where σ_{θ_t} is a permutation operation generated based on θ_t . We refer to k as the *synchronization period* (sync period). More formally, synchronization involves permuting every weight vector w'_j in θ_{sorted} according to its counterpart w_j in θ_t such that w_j and w'_j have the same *ranking* (defined in Section 3) for every j , and assign the permuted θ_{sorted} to θ_t . It is important to keep weight vectors in θ_{sorted} as always sorted, so that the permutation can be directly generated by indexing each w'_j using the ranking R_j of w_j with no extra computational overhead. Optionally, we could make a copy θ'_{sorted} before synchronization and

Algorithm 1 LaPerm

Require: Loss function L , initial weights θ_0
Require: Synchronization period k
Require: Inner optimizer Opt
 $\theta_{\text{sorted}} \leftarrow$ Sort weight vectors in θ_0
for $t = 1, 2, \dots$ **do**
 Sample mini-batch $d_t \sim D_{\text{train}}$
 $\theta_t \leftarrow \theta_{t-1} + \text{Opt}(L, \theta_{t-1}, d_t)$
 if k divides t **then**
 $\theta_t \leftarrow \sigma_{\theta_t}(\theta_{\text{sorted}})$ // Synchronization
 end if
end for

permute this copy so that θ_{sorted} is unchanged.

In essence, how exactly the magnitude of weights in θ_t have been updated by Opt is not of interest; θ_t is only considered to be a correction to the ranking of θ_0 . In other words, we extract permutations from θ_t . If the total number of training batches N and synchronization period k are chosen such that $k|N$, at the end of the training, the network’s weights are guaranteed to be $\sigma(\theta_{\text{sorted}})$, for a weight-vector-wise permutation σ .

Computational Complexity: Sorting is required to get the rankings of weight vectors at synchronization. If we use a linearithmic sorting method for weight vectors of size $\#w_j$, an inner optimizer with time complexity T , and sync period k , the amortized computational complexity for one LaPerm update is $O(T + \frac{1}{k} \sum_j \#w_j \log \#w_j)$. When k and the learning rate of the inner optimizer are chosen such that the weight distribution and range of θ_t are similar to that of the initial weights θ_0 , the performance of sorting can be improved by adopting, e.g., bucket sort, especially when weights are near-uniformly distributed. In modern DNN architectures, the average size of weight vectors are usually under 10^4 , e.g., in ResNet50 and MobileNet it is approximately 1017, and 1809, respectively.

5 Experiments: Train by Reconnect

We evaluate LaPerm by using it to reconnect randomly weighted CNNs shown in table 1 on the MNIST [19] and CIFAR-10 [16] dataset under a variety of settings. LaPerm has 2 hyper-parameters to itself: sync period k and the initial weights θ_0 . In Section 5.1, we examine how the initial weights affect its performance. In Section 5.2, we vary the size of k within a wide range and analyze its effect on optimization. In Section 5.3, based on the experiment results, we improve our hypothesis (initially stated in Section 1). In Section 5.4, we test our hypothesis as well as comprehensively assess the capability of LaPerm on training sparsely initialized neural networks from scratch. In Section 5.5, we attempt to create weight agnostic neural networks with LaPerm.

5.1 Varying the Initial Weights We train Conv7 on MNIST using different random initializations: He’s uniform U_H and normal N_H [9], Glorot’s uniform U_G and normal N_G [8]. We also train Conv7 initialized with N_H using Adam and LA in isolation. The trained weights obtained with Adam at the best accuracy are shuffled weight-vector-wisely and used as another initialization for LaPerm which we refer to as N_S . we use 5 random seeds and train the network for 45 epochs with batches of 50 with 0.95 learning rate decay. We choose $k = 20$ for LaPerm. For all experiments in this paper, LaPerm and LA use Adam as inner optimizer. Detailed settings are in Table 1 and Appendix.

The results are presented in Figure 4. While only small discrepancy is observed between the validation accuracies of LaPerm using U_H and N_H , they are constantly $\sim 0.1\%$ above that of U_G and N_G , which evidence the importance of weight value range for LaPerm to reach the last bit of accuracy. N_S performed similar to N_G until the 25th epoch where it stopped to improve. We consider the possibility of Adam over-adapting the values of weights in its training. When shuffled, it became difficult to

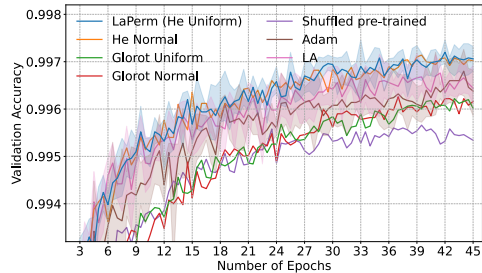


Figure 4: MNIST experiments. Text “LaPerm” is omitted except for He Uniform distribution. The band, if shown, indicates the minimum and maximum value obtained from five runs. In some cases the bands are omitted for visual clarity.

Network	MNIST Conv7	Conv2	Conv4	Conv13	ResNet50
	2x32, 32(5x5;Stride 2) 2x64, 64(5x5;Stride 2)			2x64, pool, 2x128, pool 3x256, pool	16, 16x16 16x32 16x64
Conv Layers	128 (4x4)	2x64, pool	2x128, pool	3x512, pool, 3x512, pool	
FC Layers	10	256, 256, 10	256, 256, 10	512, 10	avg-pool, 10
All / Conv Weights	325k / 326k	4.3M / 38K	2.4M / 260K	14.9M / 14.7M	760K / 760K
Epochs / Batch	45 / 50	125 / 50	90 or 125 / 50	125 / 50	200 / 50

Table 1: Architectures used in the experiments. Table is modified based on [6, 32]. Convolutional networks, if not specified, use 3x3 filters in convolutional (*Conv*) layers with 2x2 maxpooling (*pool*) followed by fully connected (FC) layers. Conv-2 and Conv-4 are identical to those introduced in [6]. Newly introduced ConvSmall is modified based on LeNet5 [18], Conv-13 is a modified VGG [28] network for CIFAR-10 adapted from [24].

rediscover the right permutation. Overall, although LaPerm pulls all the weights back to uniform random values every 20 batches ($k=20$), we see no disadvantage in its performance compared with Adam and LA. This implies that *the inner optimizer of LaPerm, between each synchronization, encode information to the weights in a manner that can be almost perfectly captured by extracting their change in rankings*. At the end, we are able to obtain state-of-the-art accuracy, i.e., $\sim 0.24\%$ test error on MNIST and slightly outperform regular optimizers.

5.2 Understanding the Sync Period k In Section 5.2, we observe when $k = 20$, LaPerm had no trouble interpreting θ_t as a permutation of θ_0 . What happens if we vary the value of k ? We train Conv4 on CIFAR-10, and sweep over 1 to 2000 for k . Hyperparameter details are in the Appendix. The results are shown in Figure 5 (a). We observe an unambiguous positive correlation between the size of sync period k and the final validation and training accuracy. Interestingly, when $k = 2000$, i.e., sync only once per two epochs, its accuracy started as the slowest but converged to the highest point, whereas for $k \leq 100$, the trend starts fast but end up with much lower accuracy. To see this clearly, in Figure 5 (b), (c), (d), we smoothed the accuracy curves and found that, before the 60th epoch (shown in (c)), the accuracies were negatively correlated with k but is reversed afterward (shown in (d)).

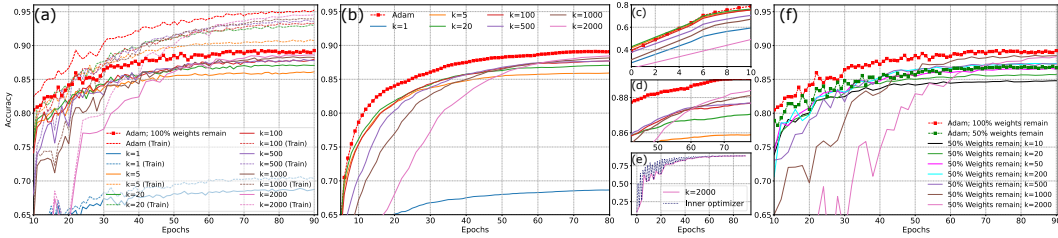


Figure 5: Conv4 on CIFAR-10. Conv4 trained for 90 epochs using batch size 50 with k chosen from $\{1, 5, 10, 20, 50, 100, 200, 500, 1000, 2000\}$. (e) shows validation accuracy of the inner optimizer at $k=2000$. In (a)~(e), Conv4 is fully initialized, i.e., 100% of weights are remained in the network. (b) is smoothed from (a). (c) and (d) are obtained by zooming in (b). (f) shows how LaPerm behaves when the initial weights are randomly pruned against different values of k . The training accuracy, if shown, are obtained by going through 30000 randomly selected training examples.

When $k=1$, LaPerm shows great degradation in its performance, which might imply that one batch update is not enough to alter the structure of weights such that the newly added information can be effectively interpreted as permutations. In contrast, in (e) for $k=2000$, sharp fluctuations are observed after and before synchronization, implies the 2000 updates of inner optimizer might have encoded an amount of information that beyond just permutations. However, we argue this extra information in the latter case is not fundamentally important, as omitting them did not have a significant negative impact on the final accuracy.

Finally, we train Conv2, Conv4, and Conv13 initialized with U_H on CIFAR-10 [16], using a batch size of 50 and compare LaPerm with Adam and LA. k is safely chosen to be 1000 for all architectures, i.e., the synchronization is done once per epoch. Other hyperparameter details are given in the Appendix.

The results are shown in Figure 6. We observe that LaPerm started slow but demonstrated a steeper growth trend in all cases. For Conv13, LaPerm outperforms Adam at its best validation accuracy.

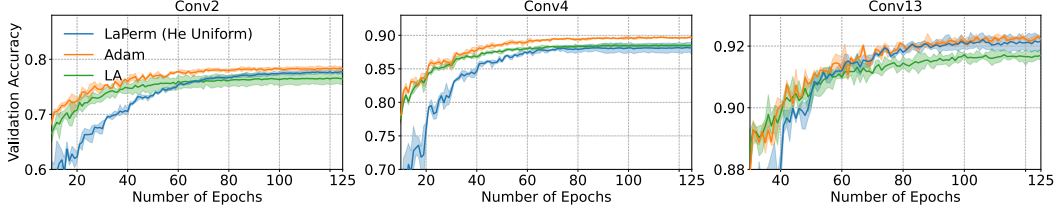


Figure 6: Validation accuracy of Conv2, Conv4, and Conv13 on CIFAR-10.

We observe a growth in LaPerm’s performance in comparison to regular optimizers as the network grows deeper. This could be partially attributed to a large number of possible permutations of weights in heavily parameterized DNNs. For a DNN with N weight vectors each of size $\#w_j$, not taking account of biases, LaPerm has access to $\prod_j^N \#w_j!$ different permutations. This number for Conv2, Conv4, Conv7, and Conv13 are approximately $10^{1.6e7}$, 10^{8e6} , 10^{8e5} and 10^{5e7} .

5.3 Two Dimensions of Weights Hypothesis Why does k have such obvious effects on training? We crystallize our observations so far, and hypothesize that neural networks trained with stochastic gradient-based optimizers are different from their random counterparts on two dimensions. D_1 : *Location of weights*, i.e., to which neurons the weights, following a certain distribution, are connected. D_2 : *Fine-tuned weight values*, i.e., the exact values of weights. Within a few steps of SGD, an iterative process where each step contributes a small amount toward the objective, the changes are simultaneously applied to both D_1 and D_2 . However, as these changes accumulate, D_1 and D_2 tend to become increasingly perpendicular.

SoWP (Section 2) epitomizes such a situation, in which the orders of weights appear to be completely separated from their values. It also implies that the statistics of D_2 within a weight matrix tend to be unified as training proceeds. These two aspects of SoWP explain why LaPerm is able to extract effective permutation when k is large. Additionally, D_1 serves as a foundation for a trained neural network to perform well, but it may or may not be immediately reflected in the accuracies. Modifying D_2 , on the other hand, can help neural networks appear to learn quickly, but without a properly learned D_1 , calibrating D_2 prematurely may introduce difficulties to improving D_1 and cause the loss to saturate at suboptimal minima. In Section 5.1, we saw how over-adapted weight values N_s performed poorly. In contrast, in Section 5.2, by setting k to extremely large, we attempted to produce SoWP so as to isolate D_1 from D_2 . Despite its efficacy, LaPerm with large k was slightly outperformed by Adam, as D_2 was not well calibrated in the end (still using uniform random values).

5.4 Reconnecting Sparsely Connected Neural Networks We further assess our hypothesis by creating a scenario in which D_1 is crucial: we let the neural network to be sparsely connected with random weights before training, i.e., many weights are zero. We expect a well-isolated D_1 to result in an effective reconnection of the neural network and guarantee its performance.

We use p to denote the percentage of initial weights that are randomly pruned, e.g., $p=10\%$ meaning 90% of weights in θ_0 are remained non-zero. We redo experiment on Conv4 as in (a) with $p=50\%$. In results on Figure 5 (f), we see that the removal of weights had no obvious negative impact on the performance, especially when k is large. In fact, performance for when $k=1000$ has improved. Next, we create a scenario in which D_2 is crucial: we perform the same random pruning as in the previous scenario; while freezing all zero connections, we train the network using Adam. In the results shown in Figure 5 (f), as predicted by our hypothesis, we observe its performance to be similar to LaPerm with $k=50$; it is clearly outperformed by LaPerm for $k \geq 200$.

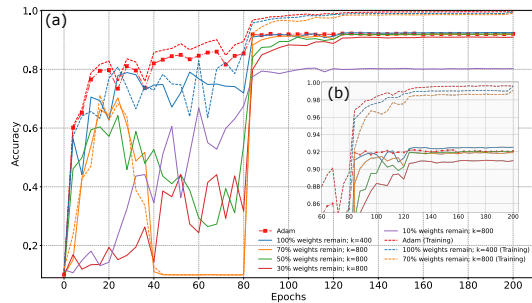


Figure 7: CIFAR-10 Validation and train accuracies of ResNet50 with different $p\%$ and k .

Since pruning 50% of weights from an over-parameterized DNN may not have a large impact on its accuracy. We test our hypothesis on ResNet50 [10] which has 760K trainable parameters (1/3 compared with Conv4). We initialize θ_0 from U_H . The learning rates of Adam for all experiments begin at 0.001 and are divided by 10 at the 80, 120, 160th epoch and by 2 at the 180th epoch. For

ResNet50 of different initial weight sparsity, we sweep over k from $\{250, 400, 800\}$ and pick the one with the best performance. More details are given in Table 1 and the Appendix.

In the results shown in Figure 7, we observe the accuracies of LaPerm when $p \in \{0\%, 30\%, 50\%, 70\%\}$ to be comparable or better than that of Adam when $p=0\%$, which again demonstrated the importance of a well-learned D_1 . Moreover, before the first learning rate drop at the 80th epoch, LaPerm appears to be extremely unstable. For $p=30\%$, LaPerm acted as if it has diverged for almost 20 epochs, but when its learning rate dropped by 10x, its train accuracy raised from 10% to 95% within three epochs. For $p=50\%$, a similar but less typical trend is observed. It might be because the progress on D_1 was not reflected in the accuracies.

Finally, we perform similar pruning experiments on all architectures in Table 1 and summarize their performance in Figure 8 using their original hyper-parameter settings. For all experiments, the weights are initialized from U_H . We sweep over a sparse grid for k from 200 to 1000 and choose the largest one that did not diverge within the first 50 epochs. Hyperparameter details are in the Appendix. We observe LaPerm, when $p \leq 70\%$, is able to achieve comparable accuracies to that of the original unpruned network. Since setting weights to zeros in a weight vector decreases the number of permutations by a factor of the factorial of the number of zeros, we expect difficulties in optimization as the number of zeros increases. On the other hand, sparsely wired DNNs allow LaPerm to trigger architectural change which adds a new dimension to the training that may have neutralized the damage of losing the permutations. Finally, since LaPerm never alters the distribution of weights, they can easily be tuned to further encode information.

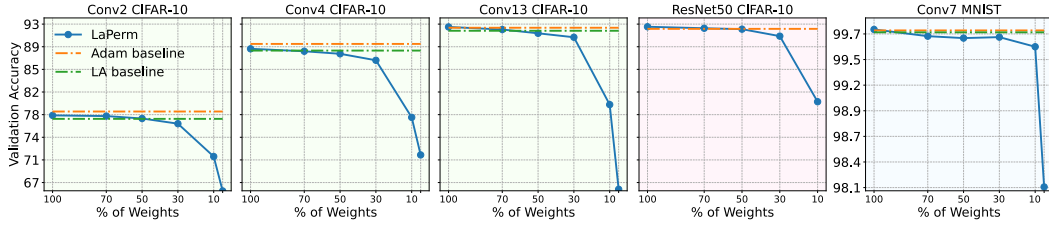


Figure 8: Randomly prune the networks before training and reconnect them using LaPerm. “% of Weights” indicates the percentage of weights remained in the network before training.

5.5 Weight Agnostic Neural networks Inspired by what [7] achieved on weight agnostic networks, we push D_1 to an extreme by setting all weights to a single shared value. We reconnect two simple networks: one without hidden layer (F_1) and one with two hidden ReLU layers of size 128 and 64 (F_2). Both networks use 10 softmax output units without bias. Since pruning is necessary for triggering architectural change, before training, 40% of weights in F_1 and on average 90% of weights in F_2 are randomly pruned. The remaining weights in F_1 and F_2 are all set to 0.08 and 0.03, respectively. We train F_1 and F_2 for 10 and 25 epochs, with batch size of 128 using LaPerm with $k=250$ on MNIST [19] for 30 random seeds each. As shown in Figure 9, we achieved $\sim 85.5\%$ and $\sim 53\%$ on F_1 and F_2 .

6 Related Work

Lottery Ticket Hypothesis Frankle et al. in [6] explored a 3-step iterative pruning strategy for finding random subnetworks which can be trained efficiently. They repeatedly train the network, prune $p\%$ of the weights, and reinitialize the remaining weights. For LaPerm, when $p\%$ of initial weights θ_0 are pruned and k is large, synchronization can be considered as finding the top $1 - p\%$ of weights in θ_t and “reinitialize” them. However, as opposed to reinitializing to their original values in θ_0 as in [6], LaPerm set them with *proper values* chosen from θ_0 that match the rankings. We have demonstrated its virtues: LaPerm is performant despite being *one-shot*, whereas the method in [6] requires heavy usage of the training data and to train from scratch for many times. In [6], the $p\%$ starts 0 and gradually increased, whereas LaPerm by utilizing the relation between D_1 and D_2 showed promising performance even when the network is already pruned before training. We plan to explore varying p during training for LaPerm in the future. Moreover, [6] proposed an untested conjecture that SGD seeks out and trains a subset of well-initialized weights. In 5, we empirically show that it is important for SGD to seek out a good D_1 which might be pointing to the same direction. Our analysis might offer a complementary perspective for evaluating their conjecture.

Random weights and Super-masks [27, 32] hypothesized and demonstrated that pruning is training. In contrast, we show that reconnecting is training. For a vector of size N , they choose from 2^N different ways of masking, whereas we explore the space of $N!$ permutations. Ramanujan et al. [27] mentioned that they could not obtain desirable performance when the network is not sparse enough or too sparse. However, by exploiting the flexibility in reconnection, we are able to achieve promising results with a wide range of sparsity. Finally, it was interesting that the best validation accuracy when $p = 50\%$ on Conv2 and Conv4 described in [27] $\sim 78\%$ and $\sim 86\%$ are similar to our results $\sim 78\%$ and $\sim 88.5\%$. It was also intriguing that the better results in [27] were obtained using *Signed Kaiming Constant* as opposed to Kaiming’s uniform [9] as we did.

Large Learning Rate and Generalization In Figure 5 (e), when Conv4 with LaPerm $k=2000$, sharp increase in accuracy is observed between synchronizations. In Section 5.4, when training ResNet50 on Cifar-10, we encountered “resurrection” in train accuracy from 10% to 95% within 3 epochs after the learning rate drop. [23] investigated a phenomenon in which large learning rate achieves better generalization soon after the learning rate is annealed. Their key insight is on how small learning rate behaves differently when encountered easy-to-generalize, hard-to-fit patterns v.s. hard-to-generalize, easier-to-fit patterns. Although we never used large learning rate but forcefully and semi-randomly regularize the weights, our hypothesis in Section 5.3 shares a similar philosophy with their insight. Drawing a connection between our work and [23] might offer an alternative perspective for understanding generalization.

Weight Agnostic Neural networks Search An interesting work by Gaier and Ha [7] creates neural networks that can perform various tasks without weight training. In Section 5.5, we made a similar attempt. Different from [7], we did not create new connections or equip neurons with different activation functions, but only reconnects basic layer-based neural networks. On MNIST, they created neuron-based architecture using fewer connections but achieved better results $\sim 92\%$ than ours $\sim 85.5\%$ may evidence the advantage of neuron-based architectures over basic layer-based ones.

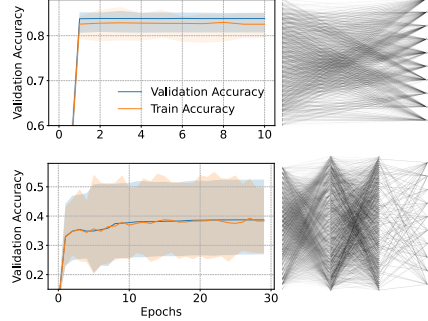


Figure 9: (left) Accuracies obtained by using LaPerm to train two networks with 0 and 2 hidden layers initialized with a single weight value on MNIST. (Right) Weight agnostic neural network obtained at their highest validation accuracies.

7 Discussion and Future Work

In this work, we explored a phenomenon of weights in SGD-trained neural networks sharing strikingly similar statistical properties, which implies an surprisingly isolable relation between the values and the locations of weights. Exploiting such property, we proposed a method to train DNNs by reconnection which has implication for both optimization and pruning. We presented a series of experiments on our method and offered a hypothesis for explaining our results.

Is SoWP necessarily desirable? We have conducted preliminary experiments under the scenario in which we force the violation of SoWP by initializing LaPerm with dissimilar weights. We observe that DNNs are still able to learn but show degraded performance. A rigorous theoretical work on SoWP would be an interesting future direction. Additionally, LaPerm can be applied like a regularization technique, i.e., it can begin and stop at appropriately chosen timing, so that it together with its inner optimizer can potentially work more flexibly. Future work could involve building schedules for the learning rate, sync period, and pruning rate. Being able to train-by-reconnect would also simplify the design of physical neural networks [26] by replacing sophisticated memristive-based neuron connections [2, 29] with fixed weight devices and permutation circuits. Moreover, a DNN trained by LaPerm can be reproduced as long as (1) a rule which is used to generate the initial weights and (2) sets of distinct consecutive integers representing a permutation is presented. We can thus store the weights using Lehmer code [20] or integer compression methods [15, 21, 22].

In this work, we have conducted experiments only on vision centric tasks on small datasets (MNIST, CIFAR-10), despite that the SoWP is also found ubiquitously in neural networks trained on larger datasets, e.g., ImageNet [5]. In future work, we plan to explore how neural networks learn when facing more challenging tasks. Finally, LaPerm involves many random jumps and restarts, while still able to properly train DNNs, we hope that our findings can benefit the understanding of DNN optimization and motivate the creation of new algorithms that are able to avoid the pitfalls of gradient-descent.

References

- [1] Martín Abadi, Ashish Agarwal, Paul Barham, Eugene Brevdo, Zhifeng Chen, Craig Citro, Greg S. Corrado, Andy Davis, Jeffrey Dean, Matthieu Devin, Sanjay Ghemawat, Ian Goodfellow, Andrew Harp, Geoffrey Irving, Michael Isard, Yangqing Jia, Rafal Jozefowicz, Lukasz Kaiser, Manjunath Kudlur, Josh Levenberg, Dandelion Mané, Rajat Monga, Sherry Moore, Derek Murray, Chris Olah, Mike Schuster, Jonathon Shlens, Benoit Steiner, Ilya Sutskever, Kunal Talwar, Paul Tucker, Vincent Vanhoucke, Vijay Vasudevan, Fernanda Viégas, Oriol Vinyals, Pete Warden, Martin Wattenberg, Martin Wicke, Yuan Yu, and Xiaoqiang Zheng. TensorFlow: Large-scale machine learning on heterogeneous systems, 2015. Software available from tensorflow.org.
- [2] Francesco Caravelli and Juan Carbajal. Memristors for the curious outsiders. *Technologies*, 6(4):118, Dec 2018.
- [3] François Chollet et al. Keras. <https://github.com/fchollet/keras>, 2015.
- [4] François Chollet. Xception: Deep learning with depthwise separable convolutions. In *Proceedings of the IEEE conference on computer vision and pattern recognition*, pages 1251–1258, 2017.
- [5] J. Deng, W. Dong, R. Socher, L.-J. Li, K. Li, and L. Fei-Fei. ImageNet: A Large-Scale Hierarchical Image Database. In *CVPR09*, 2009.
- [6] Jonathan Frankle and Michael Carbin. The lottery ticket hypothesis: Finding sparse, trainable neural networks. In *International Conference on Learning Representations*, 2019.
- [7] Adam Gaier and David Ha. Weight agnostic neural networks. In *Advances in Neural Information Processing Systems 32*, pages 5364–5378. Curran Associates, Inc., 2019.
- [8] Xavier Glorot and Yoshua Bengio. Understanding the difficulty of training deep feedforward neural networks. In Yee Whye Teh and Mike Titterton, editors, *Proceedings of the Thirteenth International Conference on Artificial Intelligence and Statistics*, volume 9 of *Proceedings of Machine Learning Research*, pages 249–256, Chia Laguna Resort, Sardinia, Italy, 13–15 May 2010. PMLR.
- [9] Kaiming He, Xiangyu Zhang, Shaoqing Ren, and Jian Sun. Delving deep into rectifiers: Surpassing human-level performance on imagenet classification. In *Proceedings of the 2015 IEEE International Conference on Computer Vision (ICCV)*, ICCV '15, page 1026–1034, USA, 2015. IEEE Computer Society.
- [10] Kaiming He, Xiangyu Zhang, Shaoqing Ren, and Jian Sun. Deep residual learning for image recognition. In *2016 IEEE Conference on Computer Vision and Pattern Recognition, CVPR 2016, Las Vegas, NV, USA, June 27-30, 2016*, pages 770–778. IEEE Computer Society, 2016.
- [11] Kaiming He, Xiangyu Zhang, Shaoqing Ren, and Jian Sun. Identity mappings in deep residual networks. In *European conference on computer vision*, pages 630–645. Springer, 2016.
- [12] Andrew G. Howard, Menglong Zhu, Bo Chen, Dmitry Kalenichenko, Weijun Wang, Tobias Weyand, Marco Andreetto, and Hartwig Adam. Mobilenets: Efficient convolutional neural networks for mobile vision applications. *ArXiv*, abs/1704.04861, 2017.
- [13] G. Huang, Z. Liu, L. Van Der Maaten, and K. Q. Weinberger. Densely connected convolutional networks. In *2017 IEEE Conference on Computer Vision and Pattern Recognition (CVPR)*, pages 2261–2269, 2017.
- [14] Sergey Ioffe and Christian Szegedy. Batch normalization: Accelerating deep network training by reducing internal covariate shift. In *Proceedings of the 32nd International Conference on Machine Learning - Volume 37, ICML'15*, page 448–456. JMLR.org, 2015.
- [15] Gonzalo Navarro Jérémy Barbay. Compressed representations of permutations, and applications. *26th International Symposium on Theoretical Aspects of Computer Science*, pages 111–122, 2009.
- [16] Alex Krizhevsky. Learning multiple layers of features from tiny images. Technical report, 2009.
- [17] Anders Krogh and John A. Hertz. A simple weight decay can improve generalization. In J. E. Moody, S. J. Hanson, and R. P. Lippmann, editors, *Advances in Neural Information Processing Systems 4*, pages 950–957. Morgan-Kaufmann, 1992.

- [18] Y. Lecun, L. Bottou, Y. Bengio, and P. Haffner. Gradient-based learning applied to document recognition. *Proceedings of the IEEE*, 86(11):2278–2324, 1998.
- [19] Yann LeCun, Corinna Cortes, and CJ Burges. Mnist handwritten digit database. *ATT Labs [Online]*. Available: <http://yann.lecun.com/exdb/mnist>, 2, 2010.
- [20] Derrick Henry Lehmer. Teaching combinatorial tricks to a computer. *Sympos. Appl. Math. Combinatorial Analysis, Amer. Math. Soc.*, (10):179–193, 1960.
- [21] Daniel Lemire and Leonid Boytsov. Decoding billions of integers per second through vectorization. *arXiv e-prints*, page arXiv:1209.2137, September 2012.
- [22] Daniel Lemire, Leonid Boytsov, and Nathan Kurz. SIMD Compression and the Intersection of Sorted Integers. *arXiv e-prints*, page arXiv:1401.6399, January 2014.
- [23] Yuanzhi Li, Colin Wei, and Tengyu Ma. Towards explaining the regularization effect of initial large learning rate in training neural networks. In *Advances in Neural Information Processing Systems*, pages 11669–11680, 2019.
- [24] Shuying Liu and Weihong Deng. Very deep convolutional neural network based image classification using small training sample size. *2015 3rd IAPR Asian Conference on Pattern Recognition (ACPR)*, pages 730–734, 2015.
- [25] Alex Nichol, Joshua Achiam, and John Schulman. On first-order meta-learning algorithms. *CoRR*, abs/1803.02999, 2018.
- [26] Alex Nugent. Physical neural network design incorporating nanotechnology, May 3 2005. US Patent 6,889,216.
- [27] Vivek Ramanujan, Mitchell Wortsman, Aniruddha Kembhavi, Ali Farhadi, and Mohammad Rastegari. What’s hidden in a randomly weighted neural network? *arXiv preprint arXiv:1911.13299*, 2019.
- [28] Karen Simonyan and Andrew Zisserman. Very deep convolutional networks for large-scale image recognition. In Yoshua Bengio and Yann LeCun, editors, *3rd International Conference on Learning Representations, ICLR 2015, San Diego, CA, USA, May 7-9, 2015, Conference Track Proceedings*, 2015.
- [29] G. Snider. Self-organized computation with unreliable, memristive nanodevices. *NANOTECHNOLOGY Nanotechnology*, 18:365202–13, 09 2007.
- [30] Nitish Srivastava, Geoffrey Hinton, Alex Krizhevsky, Ilya Sutskever, and Ruslan Salakhutdinov. Dropout: A simple way to prevent neural networks from overfitting. *J. Mach. Learn. Res.*, 15(1):1929–1958, January 2014.
- [31] Michael Zhang, James Lucas, Jimmy Ba, and Geoffrey E Hinton. Lookahead optimizer: k steps forward, 1 step back. In *Advances in Neural Information Processing Systems 32*, pages 9597–9608. Curran Associates, Inc., 2019.
- [32] Hattie Zhou, Janice Lan, Rosanne Liu, and Jason Yosinski. Deconstructing lottery tickets: Zeros, signs, and the supermask. In *Advances in Neural Information Processing Systems 32*, pages 3597–3607. Curran Associates, Inc., 2019.
- [33] Barret Zoph, Vijay Vasudevan, Jonathon Shlens, and Quoc V. Le. Learning transferable architectures for scalable image recognition. *2018 IEEE/CVF Conference on Computer Vision and Pattern Recognition*, Jun 2018.

A Appendix

A.1 Contents of the Supplementary materials

In addition to what is included in this Appendix, the supplementary material repository also includes the code and pre-trained weights. Detailed example usages of the code, e.g., training and validation script for reproducing the main results of the paper, are also included. Table of contents and the explanations for the usage are described in `README.md` in the supplementary materials. **The supplementary material is currently not available for this preprint.**

A.2 Supplementary Materials for Section 2: Similarity of Weight Profiles

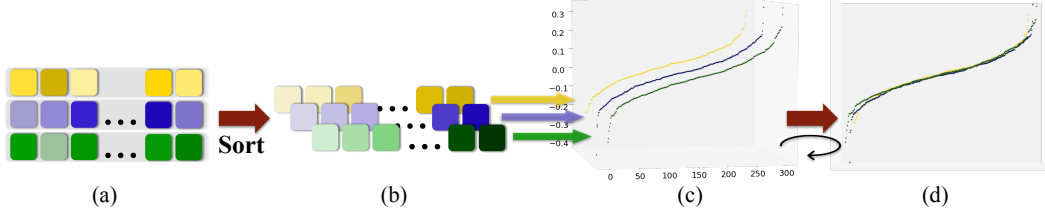


Figure 10: How to plot weight profiles. (a) Given weight vectors. (b) Sort each weight vector ascendingly. (c) Plot a scatter plot for each weight vector. (d) Hide the z-axis. For the definitions of terms please refer to Section 2.

Complementary to Section 2, we present the weight profiles of pre-trained convolutional neural networks on ImageNet [5] including VGG16 [28], VGG19 [28], ResNet50 [10], ResNet101 [10], ResNet152 [10], ResNet152-V2 [11], DenseNet121 [13], DenseNet169 [13], DenseNet201 [13] Xception [4], NASNet-Mobile [33], and NASNet-Large [33]. The pre-trained weights of the aforementioned neural networks are downloaded directly from `keras.applications` [3]. Since compiling all the weight profile images into one file may harm the reading experience, we only show the weight profile of DenseNet121 here and store the rest of images in a folder named `weight_profiles` included in the supplementary materials.



Figure 11: DenseNet121. The image can be zoomed in for details.

A.3 Supplementary Materials for Section 3: Is Permutation the Essence of Learning?

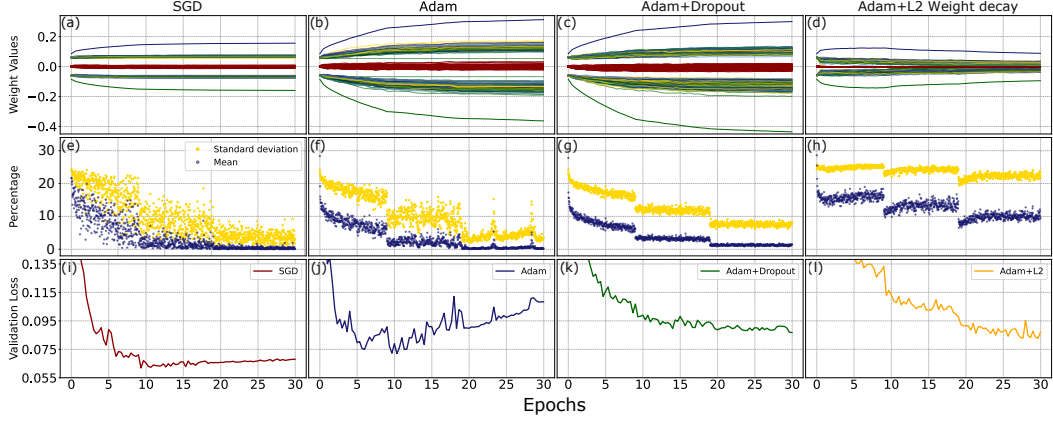


Figure 12: Monitoring weight distributions, changes in the ranking distance (permutations), and validation loss in the first weight matrix of the network. Each column title indicates the experiment setting. Under each title from the top to bottom shows the evolution of: (Row 1) the weight distributions shown as {15, 50, 85}th percentiles. Each percentile is displayed as 100 lines representing all 100 weight vectors. The 50th percentile is highlighted using red color. The maximum and minimum weights are shown as single lines above and under the percentiles, respectively. (Row 2) ratio of the mean and standard deviation of the ranking distance to the size of the weight vector, i.e., $\overline{D}_t/784$ and $SD[D_t]/784$. (Row 3) the trend of validation loss on 10,000 test images.

Experiment settings We train a fully-connected DNN with 2 hidden layers (100 ReLU units each) and an output layer with 10 softmax units using the cross-entropy loss on MNIST [19]. The network is initialized with uniform random weights as introduced in [9] and is trained on 60,000 training examples for 30 epochs with 50 examples per mini-batch. The network is validated on 10,000 test examples. The learning rates in all experiments are divided by 2 and 5 at the 10th and 20th epochs. In isolation, we train using the same architecture and initialization under four different settings: (1) SGD (initial learning rate: $1e-1$) with no regularization. (2) Adam (initial learning rate: $1e-3$) with no regularization. (3) Adam (initial learning rate: $1e-3$) with 0.4 and 0.3 dropout [30] on the outputs of the first and second hidden layers. (4) Adam (initial learning rate: $1e-3$) with $2e-4$ L2 weight decay [17] on the weights associated with the first and second hidden layers.

Analysis We first study the evolutions of weight distributions in Figure 12 (a)~(d) and (i)~(l). The most noticeable distinction is spotted between (b) and (d), wherein (b) the distribution expands but in (d), due to weight decay, it collapsed. On the other hand, (a) in comparison to (b) shows much less expansion. This is likely because the gradient updates of SGD tend to be scaled uniformly toward every dimension. A simplified example could be: If we uniform-randomly update a uniformly distributed initial weight matrix for n iterations, the resulting weight matrix would possess the properties of an Irwin-Hall distribution in which the standard deviation grows asymptotically to \sqrt{n} . Assuming that the updates in the actual training are sparse and their values are small, 30 epochs (with learning rate decay) would have a comparatively insignificant effect on the weight distribution. However, what we could gain from (a)~(d) is limited, e.g., despite demonstrating drastically different behaviors in validation losses in (j) and (k), (b) and (c) showed subtle differences.

Next, we study the statistics of ranking distances in Figure 3 (e)~(h). We observe that the mean distance, which is positively correlated with the total amount of changes in ranking, might signify the intensity of learning. For example, overall, (h) maintains a larger but more fluctuating mean of distance in comparison to (d), which corresponding loss curve in (l) appears to be steeper and more unstable in comparison to (k). By contrast, when the network enters the phase where only a few permutations happen, we observe a flatter loss curve and milder fluctuations, signifying the learning is nearly saturated. For example, in (i) and (k) after the 20th epoch. Moreover, we notice that during such a saturated phase, any sharp jump in the mean of distance could be a sign of overfitting. We consider the possibility that the network has encountered training examples which, according to its current knowledge, are outliers, despite these examples were presented to the network many times in the past epochs. Such sudden jumps could suggest that the network begin to fit the rest

of the examples too well. As a result, more permutations are triggered to cope with such outliers, which resulted in further overfitting. (f) and (j) epitomize such situation: At around the 24th and 30th epochs, the sharp rise in the mean of ranking distance predicted the deterioration in validation loss, without any knowledge about the validation data.

Moreover, the behaviors of permutations showed unique traits under different settings. For setting (1), the trends seem highly random, especially at learning rate $= 0.1$. This is expected, because SGD uses the update rule: $\theta \leftarrow \theta - \alpha \cdot \nabla_{\theta} L(\theta, d)$ for learning rate α , weights θ , and loss function L , and thus the update happens at each step is largely dependent on the randomly sampled batch d . In contrast, in (f)~(h), i.e., the permutations caused by Adam with or without regularization, appear to be much less random. This has to do with its update rule: $\theta \leftarrow \theta - \alpha \cdot m / \sqrt{v}$, where m and v are dependent on all previous gradients since the beginning of training, and thus, given properly chosen hyperparameters, its behavior is not dominated by the randomness in training. Moreover, comparing (f) with (g), we see that dropout let Adam create, on average, larger and more stable sized updates. Since dropout is equivalent to training different randomly sampled sub-networks, neurons are constantly placed in an environment where frequent self-correction is necessary. Finally, when L2 weight decay is applied, the changes in ranking tend to be great in both its numbers and sizes. This can be observed from (d) where the weight distribution collapses due to the L2 weight penalties, i.e., the weights, on average, are becoming closer to each other. The closer two weights are from each other, the easier their rankings can be swapped and the larger ranking distance the swap would cause by an update.

In conclusion, stochastic gradient-based optimizers are not only permuting the weights, as we also observe frequent changes in the statistics of weights. Nevertheless, within these noisy fluctuations, we can distill substantial progress of learning by only looking at the relative ranking of the weights.

A.4 Supplementary Materials for Section 4: Lookahead Permutation (LaPerm)

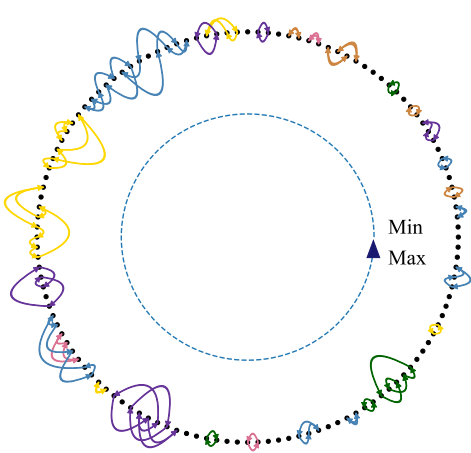


Figure 13: Permutations between the first two LaPerm (use Adam as inner optimizer, $k = 20$) iterations on a weight vector of size 128 in a convolutional neural network trained on the CIFAR-10 dataset. Vertices (black dots) representing the 128 weight values are aligned counterclockwise in a circle in ascending order. Each disjoint permutation cycle is marked using the same color.

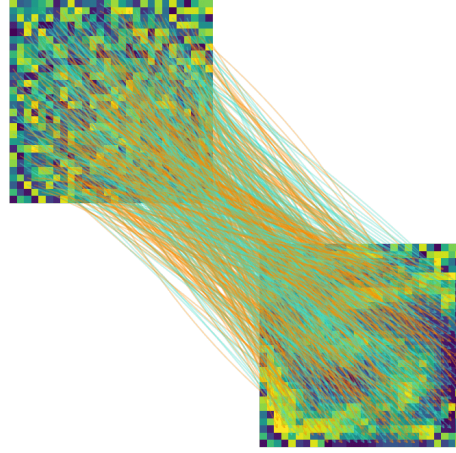


Figure 14: A fully connected neural network with one hidden layer is trained on MNIST [19]. One typical weight vector associated with the hidden layer before (upper left) and after training (lower right) using permutation. The same weights are connected using an arrow of color green or orange chosen at random.

If necessary, we could accurately extract the permutations performed by LaPerm by directly comparing the rankings of weights between two consecutive synchronizations and deduce the permutations using a cycle finding algorithm. Since permutation graphs are perfect, we could adopt simple algorithms such as DFS to efficiently find them. A visualization of such permutations is shown in Figure 13. More intuitively, since the weight vector after training using LaPerm is a direct permutation of the original random vector, we visualize this relationship in Figure 14.

A TensorFlow [1] implementation of LaPerm is included in the supplementary material. Please refer to A.1 for more details.

A.5 Supplementary Materials for Section 5: Experiments: Train by Reconnect

We described extra experiment details that are not mentioned in Section 5. The complete visual-based architecture descriptions for all the neural networks used in this paper are included in the folder named `networks`. The train and evaluation scripts are also included in the supplementary material, please refer to A.1 for more details. Note that the accuracies for LaPerm for all experiments are calculated right after synchronization.

A.5.0 Improve the Experiment Results The focus of our paper was not on pursuing the state-of-the-art accuracies, but understanding the effectiveness of a well-learned D_1 and its possible implication on optimization and pruning. Therefore, we chose straightforward experiment settings for clear demonstrations. However, the experiment results described in Section 5 can be further improved if we refine the hyperparameters. We demonstrate the following examples.

For the last experiment in Section 5.4, we chose $k \leq 1000$ from a sparse grid and obtained results in Figure 8. However, better value of k exists, e.g., when $k=2000$ (using the same hyperparameters settings) as demonstrated in Figure 15, we are able to achieve a better result compared to what was mentioned in Section 5.4. We expect that a fine tuned k or a schedule designed for k can further improve the performance of LaPerm.

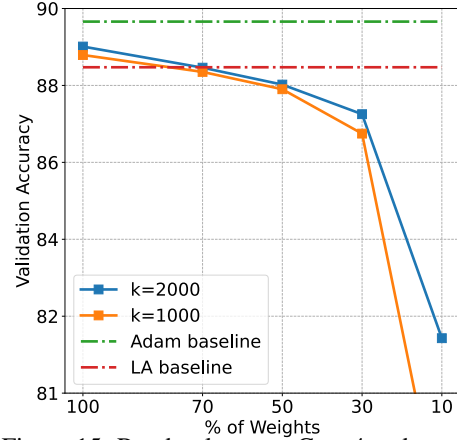


Figure 15: Randomly prune Conv4 and reconnect it using LaPerm with $k=1000$ and 2000 . “% of Weights” indicates the percentage of weights remained.

In Section 5.5, we used the same pruning rate for all three weight matrices of F_2 (hyperparameter details in Appendix A.6.4). However, since there are 100352, 8192, and 640 parameters in its weights matrices, respectively, a simple way to improve pruning without introducing extra complexity would be to prune while considering the number of parameters, e.g., heavily parameterized matrices should be pruned more. We reconduct the experiment and randomly prune the three weight matrices of F_2 at the rates of 93%, 86%, and 67%, respectively (7%, 14%, and 33% of weights remain nonzero). We achieved test accuracy of 78.14%, which is much higher than the result mentioned in 5.5, i.e., ~53%. Note that the results of all other pruning experiments, e.g., in Section 5.4, can be potentially improved by taking into account the size of weight vectors while setting the pruning rate, as opposed to using the same pruning rate for all layers.

A.5.1 General Information about the Datasets In this paper, we considered classifying images in the MNIST [19] and CIFAR-10 [16] datasets. The MNIST dataset consists of 70,000 black and white images of size 28×28 with 10 different categories. The CIFAR-10 dataset consists of 60,000 colored images of size 32×32 , with 10 different categories.

A.5.2 Experiment Details for Section 5.1 Varying the Initial Weights For MNIST, we normalize both train and test data and use real-time random data augmentation with rotation up to 10 degrees, width and height shifts up to 10% of the original image size for train data, and random zoom at a range of 10%. The learning rate for Adam (both as an individual optimizer and inner optimizer) starts with $1e-3$ and is multiplied by 0.95 at the end of each epoch. For LA, we use TensorFlow’s [1] default settings, i.e., sync period 6 and slow step size 0.5. The networks are trained on 60,000 sample images and validated on 10,000 test images. For Conv7, no regularization except dropout [30] is used.

A.5.3 Experiment Details for Section 5.2 Understanding the Sync Period k For CIFAR-10, we z-score normalize (subtract by mean and divide by standard deviation) all images, and use real-time random data augmentation with rotation up to 15 degree and width and height shifts up to 10% of the original image size and random horizontal flip. The networks are trained on 50,000 training images and validated on 10,000 test images. For all experiments on Conv2, Conv4, and Conv13 in this section, we use a L2 weight decay of rate $1e-4$, dropout[30], and batch normalization[14]. The batch

normalization [14] layers are updated regularly using the inner optimizer of LaPerm. Adam (both as an individual optimizer and inner optimizer) use an initial learning rate of $1e-3$, and is multiplied by 0.6 at every 10th epoch.

A.5.4 Experiment Details for Section 5.4 Reconnecting Sparsely Connected Neural Networks

We apply the same data preprocessing, data augmentation, and train-validation split as in the previous section. For Conv2, Conv4, and Conv13 we use the same regularizations and training hyperparameters as in the previous section. For ResNet50, the learning rates of Adam (both as an individual optimizer and inner optimizer) begin at $1e-3$ and are divided by 10 at the 80, 120, 160th epoch, and by 2 at the 180th epoch.

Since the input layer usually has significantly fewer weights in each weight vector, to avoid creating bottlenecks, the input layer is always pruned only up to 20% (at most 20% of weights are set to zero), whereas the rest of layers share the same rate of pruning as described in the paper. The batch normalization layers and biases (Conv7) are not pruned.

A.5.5 Experiment Details for Section 5.5 Weight Agnostic Neural Networks

For the experiments in the section, we perform the same data normalization as mentioned in A.4.1, but do not use data augmentation. For both experiments, we use an initial learning rate of $1e-3$ and multiply it by 0.95 at each epoch. For F_1 , we do not use regularization. For F_2 , we use L2 weight decay of rate $1e-4$ on the hidden layers. The weight matrix of F_1 is randomly pruned by 40% (40% of weights are set to zeros). The weight matrices of F_2 are randomly pruned by 90%.